TCAD Simulations of High-Aspect-Ratio Nano-biosensor for Label-Free Sensing Application

Rakshita Pritam Singh Dhar[1*], Naveen Kumar[1*], Cristina Medina-Bailon[1], César Pascual García[3], Vihar Petkov Georgiev[1*]

[1]Device Modelling Group, James Watt School of Engineering, University of Glasgow, UK

[2]Nano-Enabled Medicine and Cosmetics group, Materials Research and Technology Department, Luxembourg Institute of Science and Technology (LIST), Belvaux, Luxembourg

*Correspondence: r.dhar.1@research.gla.ac.uk, Naveen.Kumar@glasgow.ac.uk, Vihar.Georgiev@glasgow.ac.uk

***Abstract*- In this paper, we are presenting simulations of junctionless ion-sensitive field-effect transistor (JL-ISFET) as a pH sensor. Our approach is based on a combination of analytical and numerical methods to reveal the impact of the device geometry and structure on its performance. To have a realistic representation of the fabricated device, further simulations are carried which portray the sensing of surface potential by introducing interface trap charges between the oxide layer and electrolyte. Here, we present our initial steps that belong to a more complex and physically more elaborate simulation framework, which will lead to a better device sensing and fabrication choices of more generic biosensors, in a transition from analytical models to numerical simulations to include effects such as surface roughness and defects in the oxide.**

Keywords- ISFET, TCAD simulation, Electrolyte modelling.

I. INTRODUCTION

In the early stages, biosensors based on field-effect transistors (FETs) were fabricated with large planar architectures using heterojunctions which permitted only one-dimensional diffusion of the analytes towards the sensor. However, in the last decade, the progress of the technology and fabrication capabilities in the semiconductor industry allows us to use novel techniques to complete transistors with nanoscale non-planar configuration involving the diffusion of analytes in three-dimensions.

Ion-sensitive field-effect transistors (ISFETs) are devices, initially used as pH sensors, which can also be used to detect different biomolecules using certain modifications. Junction-FET sensors become less reliable with miniaturization due to reduced gate control and complex fabrication process, leading to the development of junctionless transistors. A junctionless (JL) transistor is a device that has uniform doping concentrations throughout the source, channel and drain. Junctionless transistors suffer from a higher threshold voltage that can be tweaked with the use of gate-all-around architecture. In all cases, the limits of detection depend on the diffusion of analytes and the equilibrium of charges at the interface between the liquid and solid phase. The miniaturization of the devices contributes to a more efficient diffusion of the analytes towards the sensing surface, leading to faster adsorption of the biomarker molecules at the surface of the sensor, while the 3D gating present in nanowires contributes to better transduction [1]. As a result, the sensors can detect lower concentrations in the electrolyte being more sensitive to the changes in the solution. The principle was first applied with silicon nanowires [2], which provided a leap in the limits of detection [3]. However, variability and reliability issues of the sensors have hindered their reach to clinical applications. The variability and the reliability could be improved by using larger devices based on FinFET technology made on silicon-on-insulator (SOI). It is possible to fabricate a high aspect ratio (height>>width of the device) FinFETs, which allows an increase in the total surface area thereby improving the reliability of bio-functionalization and the sensitivity of the sensor [4] [5], while keeping the advantage of 3D gating. Thus, FinFET based JL-ISFETs provides better gate controllability without compromising the ease in fabrication. These kind of ISFETs have great compatibility with the CMOS technology. Nevertheless, there are still challenges to be tackled related to optimisation of the device's architecture and materials chosen [6] [7].

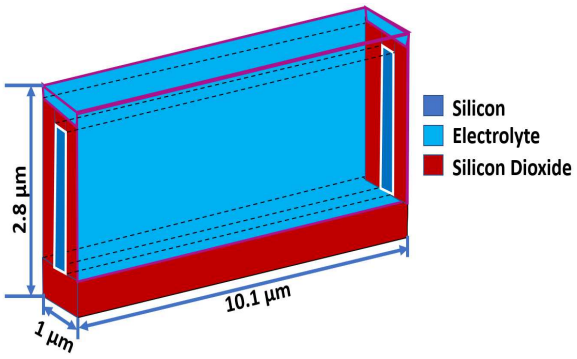

Fig. 1 Schematic of the device implemented in our simulation domain which is based on high-aspect-ratio (height >> width of the device) junctionless ion-sensitive field-effect transistor (JL-ISFET). White rectangular boxes shown on the sides are source/drain electrodes (side contacts).

In this work, we have performed a numerical design-of-experimental (DoE) study to improve the device design based on junctionless ion-sensitive field-effect transistor (JL-ISFET) based on FinFET technology. We have performed device simulations using Synopsys Technology Computer-Aided Design (TCAD) program Sentaurus. Based on the TCAD simulations, current-voltage characteristics (I_D-V_G curve) for p-type FinFET of the device, which are the transfer characteristics of the varying pH response, are obtained explaining the matching behaviour to experimental fabrication data [4]. In our case, we have used the interaction of ions with the oxide surface as an indicator of pH, with the objective in the future, to model other more complex interface functionalization. pH is already meaningful because pH-ISFET technology is widely used.

II. DEVICE ARCHITECTURE AND MATERIAL PROPERTIES

Fig. 1 shows schematics of a high-aspect-ratio JL-ISFET device considered in this work. The pink contour in Fig. 1 is the boundary condition where the gate voltage V_G is applied and the white contours in Fig. 1 correspond to contacts where the drain-source bias, V_{DS} is applied. The implemented geometry and dimensions are based on a fabricated device [4]. The simulation domain has the following dimensions of length, height, and width 10.1µm, 2.8µm and 1µm, respectively. The device has a silicon channel with a width of 200nm and an oxide thickness of 5 nm/10 nm, respectively. In this work, the JL-ISFET is designed to have a high-aspect-ratio meaning the height to width ratio of the fin is very high (h: w ≈10). This ratio allows for a larger total surface area.

Our simulations are based on two types of device configurations. The first one is a JL-ISFET device with a dry gate (a MOSFET device without electrolyte in the gate) and the second one is a JL-ISFET device with an electrolyte. The electrolyte considered in our work is NaCl+H_2O. The channel is p-type doped Si (boron atoms for doping) with a concentration of $10^{17}cm^{-3}$. Furthermore, the simulation domain includes an oxide layer which can be either hafnium dioxide or silicon dioxide and the electrolyte layer which surrounds the Si channel on the three sides.

III. RESULTS AND DISCUSSIONS

Based on our simulation, we can calculate device transfer characteristics such as drain current vs. drain voltage (I_D-V_G) for each device. Fig. 2 shows the I_D-V_G curve of the JL-ISFET with a dry gate. Four types of devices are considered having two different oxide thicknesses (t_{ox}) and two oxide materials, respectively. According to MOS equation [8], I_D is directly proportional to permittivity (ε_0) and inversely proportional to t_{ox}. Since HfO_2 has a very high dielectric constant (ε~20) in comparison to SiO_2 (ε = 1) [9], this leads to high C_{ox} for the I_D at V_G = -1V. Thinner oxide values cause higher values of the drain current, hence the devices with t_{ox}=5 nm have high I_D compared to transistors with t_{ox}=10nm. At V_G = 0 V, there is weak depletion of the hole carriers due to gate metal work-function which leads to less hole current in the channel. For V_G > 0V, the depletion is more, and it will affect the most on the 5nm HfO_2 device, leading to the lowest drain current.

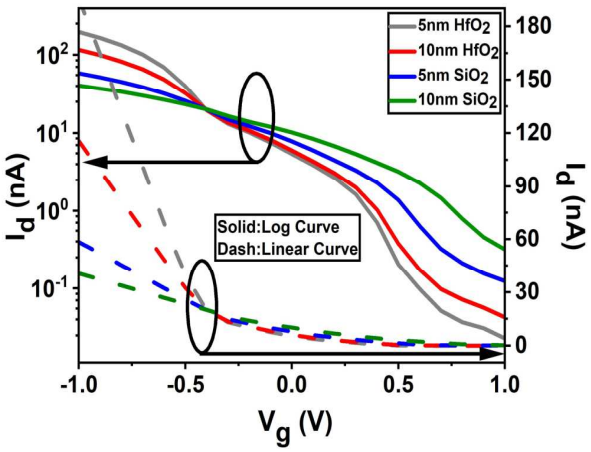

Fig. 2 Current-Voltage (I_D-V_G) characteristics of four different MOSFET devices (without electrolyte in the gate). The device dimensions are the same except the thickness and the type of the gate oxide.

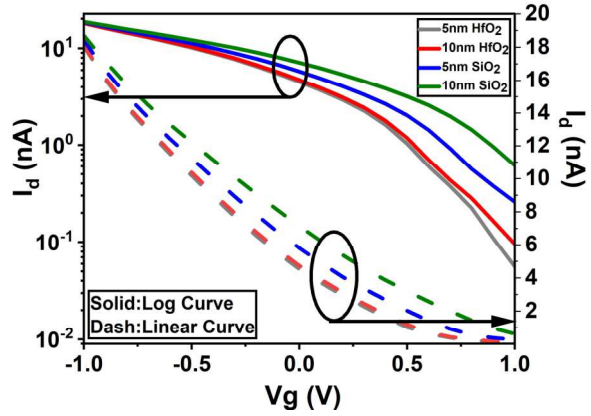

Fig. 3 Current-Voltage (I_D-V_G) characteristics of the different devices with a with an electrolyte [pH @ isoelectric point] above the gate oxide. The device dimensions are the same except the thickness and the type of the gate oxide.

A. Defining Electrolyte in TCAD

As a next step, we have introduced an electrolyte on the top of the gate oxide to simulate the solvent in the biosensor. The electrolyte is modelled as stated in [10]. The electrolyte which is an ionic solution is modelled as a semiconductor material having a dielectric constant of water (ε_r=80) [10]. The electrolyte's charge distribution is represented by the Poisson-Boltzmann equation which is close to the semiconductor equation. By changing the mobility of holes and electrons of the semiconductor, the salt concentration in the solution has been simulated. The electron mobility has a value set to Cl^- ions in water ($6.88*10^{-4}\ cm^2V^{-1}s^{-1}$) and the hole mobility is set to value of Na^+ions in water ($4.98*10^{-4}\ cm^2\ V^{-1}s^{-1}$). The bandgap in the electrolyte is kept as 1.5eV to represent a solvent [11]. The applied gate bias is kept less than the voltage responsible for the electrolysis of water.

Fig. 3 shows the I_D-V_G curve for all the herein considered devices in which the electrolyte is included considering at equilibrium state (Isoelectric Point), in contact with the gate oxide. In Fig. 3, it is shown that all devices have similar ON-current amongst them [8]. The capacitance of the oxide layer (C_{ox}) varies for different devices and the capacitance of electrolyte)remains the same for all four devices. Our sytem can be described as two series capacitors where one of the capacitors takes into account the charge across the gate oxide and the other capacitor represents the charge accumulation in

the electrolyte as shown in the equation below:

$$\frac{1}{C_{eq}} = \frac{1}{C_{ox}} + \frac{1}{C_{electro}} \quad (1)$$

Where C_{eq}= equivalent capacitance of the device, C_{ox}= Oxide capacitance and $C_{electro}$= Electrolyte capacitance. In such a configuration, the dominant factor, which will determine the device behaviour, is the capacitor with the lowest value. The variation of the gate bias inverts the channel of every device with different oxide material or thickness at the highest negative value. The depletion of the channel is more prominent for the HfO_2 as compared to the SiO_2 for the highest positive gate bias. The devices with a thinner gate oxide and higher dielectric permittivity can comprehend better the ions variation in electrolyte onto the channel.

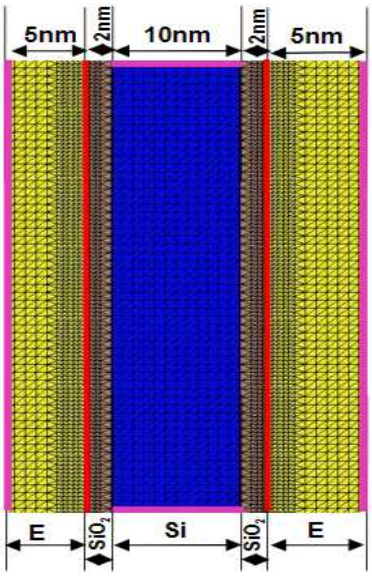

Fig. 4 2D simulation domain of the adopted ISFET device structure. Si channel is represented with a blue rectangle and has 10nm width. SiO_2 which is marked in brown has 2nm thickness and the electrolyte is depicted in yellow, and it has thickness of 5nm. The red line between the SiO_2 and the electrolyte is the place where the interface trap charges (ITC) are distributed. The pink contours are boundary conditions for the gate voltage (V_G) on both sides of electrolyte and on the top and bottom of Silicon channel are the contacts for V_{DS}.

The next step in our simulation approach is to modify the simulation domain to include pH dependence in the electrolyte section. In order to simulate the effect of the pH on the device performance, we have introduced interface trap charges (ITCs) between the gate oxide and the electrolyte. Moreover, we have modified the simulation domain from 3D to 2D. Moving from 3D to 2D device simulation domain is justified due to the high-aspect-ratio of the devices. As a first approximation, our device can be described as a transistor with gates on both sides and the top gate can be ignored due to significantly smaller surface area in comparison to the side gate area. Fig. 4 reveals the 2D simulation domain that we have adopted for further DoE investigation to save computational time. As a result, the output current will change but the surface potential will be very similar to the full 3D structure.

IV. ANALYTICAL MODEL OF OXIDE AND ELECTROLYTE

When the electrolyte is added on top of the oxide layer, a built-in potential is developed at the interface between oxide and electrolyte called the sensing surface. To represent the built-in potential at the sensing surface in TCAD simulations, ITCs are introduced (red line on Fig. 4). From a simulation perspective, changes in the values of the ITC density will directly correspond to specific values of pH in the electrolyte. Hence, it is important to be able to evaluate the exact amount of charges on the sensing surface. In order to calculate the ITC density, we have adopted the following analytical model. At 25^0C in pure water $[H^+]=[OH^-]=10^{-7}$mol/L. The Avogadro constant $N_A = 6.022*10^{23}$ mol^{-1} is converted to 1 mol/L = $6.022*10^{23}$/L = $6.022*10^{20}cm^{-3}$. For electrolyte having pH = 7, the concentration of $[H^+]$ ions = 10^{-7} mol/L which corresponds to p = $10^{-7}*6.022*10^{20}$ cm^{-3} = $6.022*10^{13}$ cm^{-3}. The hole density of states (N_V) can be calculated using equation below [11]:

$$p = N_v\, e^{-\frac{Ef-Ev}{kT}} \quad (2)$$

with a result of $2.33*10^{26}$ cm^{-3}. The same calculation can be done for the electron density of states (N_c) using the number of electrons (n) in the following equation [10]:

$$n = N_C\, e^{-\frac{Ec-Ef}{kT}} \quad (3)$$

with a result of $2.33*10^{26}$ cm^{-3}. The values of the ITC are calculated by representing the built-in potential using the equivalent surface charge density. The surface potential variation with respect to pH is given in equation below [12]:

$$\frac{\partial \Psi_0}{\partial pH} = -2.303\frac{k_B T}{q}\alpha \quad (4)$$

where Ψ_0 is the surface potential, k_B is the Boltzmann constant, T is the temperature, q is the electron charge, and α is the sensitivity parameter. α is 1 for the ideal device. The value of α is given by the equation below [12]:

$$\alpha = \frac{1}{1 + 2.303\frac{k_B T\, C_{diff}}{q^2 \beta_{diff}}} \quad (5)$$

where C_{diff} is the diffusion capacitance and β_{diff} is the intrinsic buffering capacitance. C_{diff} depends on electrolyte properties which consider double layer and stern capacitances and β_{diff} depends on the density of surface functionalization [13]. The relation between surface potential (Ψ_0) and the surface charge density (σ_{DL}) is given by equation below [12]:

$$\sigma_{DL} = Q_0 \sinh\left(\frac{q\Psi_0}{2k_B T}\right) \quad (6)$$

where $Q_0 = \sqrt{8k_B T \varepsilon_w I_0 N_{avo}}$, I_0 is the ionic concentration, ε_w is permittivity and N_{avo} is Avogadro number. The potential obtained from Eq. 4 is substituted in Eq. 6 to obtain σ_{DL} which is the ITC density (in cm^{-2}) [14]. Based on the analytical model described above, we have calculated the correlation between pH in the electrolyte as a function of the ITC density. The corresponding relationship is presented in Fig. 5 where we can observe the following two main points. First, the curve is highly non-linear, and it has a minimum at around pH=2. The reason for this is that at pH=2, all charges at the oxide-electrolyte interface are canceled (balanced) by the charges in the electrolyte. This point is known in the literature as a point-of-zero-charge (pH_{PZC}) or the isoelectric point and for SiO_2, i.e., is equal to pH=2, and the pH_{PZC} is specific for every oxide.

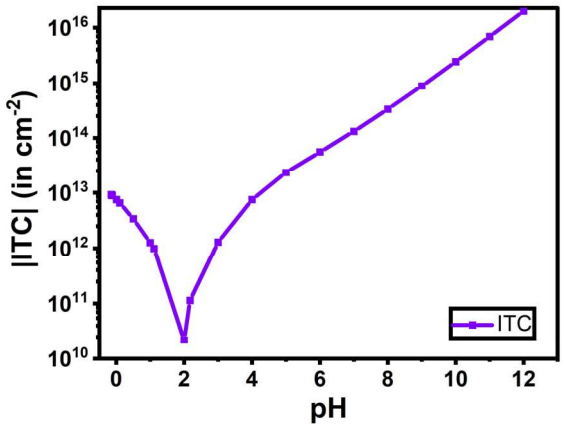

Fig. 5 Relationship of the pH values as a function of the interface trap charge (ITC) density. The data is reported in semi-log scale.

Second, for pH values between 2 and 4, the curve rises steeply for pH values close to the isoelectric point and then increases steadily. For example, at pH=5, the ITC density is $5*10^{13}$ cm^{-2}, while at pH=11 the ITC density is almost 10^{16} cm^{-2}. Hence, ITC density changes around 3 orders of magnitude for 6 values of pH which indeed is a significant change. Based on the results presented in Fig. 5, we have calculated the device behaviour. Fig. 6 shows the I_D-V_G curve of the ISFET varying the pH values from 5 to 11. As the pH increases from 5 to 11, the drain current I_D for a particular value of V_G also increases which is linked to a change of the threshold voltage for each pH.

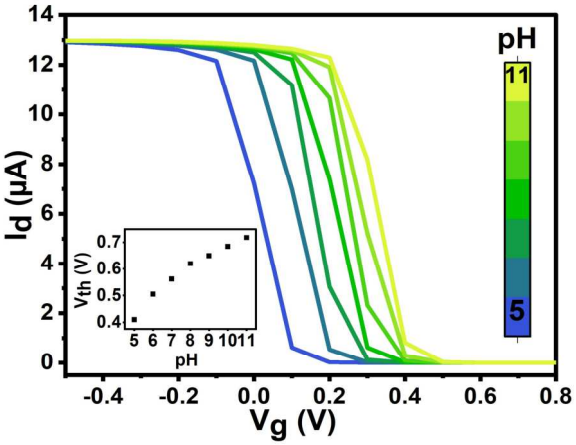

Fig. 6 Current -Voltage (Id-Vg) characteristics as a function of pH for an ISFET device. The pH varies from 5 to 11 which is represented with a blue and yellow line on the graph correspondingly.

Finally, the observed device behaviour in Fig. 6 can be explained in the following way. When the V_g has higher negative values, the I_d is saturated as the channel is inverted and when V_g holds higher positive values, the drain current decreases as the channel gets depleted. In general, higher values of pH mean lower proton concentration (positive charges) in the electrolyte. For e.g., pH = 1 means $[H^+]= 10^{-1}$ mol/L, $[OH^-] =10^{-13}$ mol/L similarly pH = 10 means $[H^+] = 10^{-10}$ mol/L, $[OH^-] =10^{-4}$ mol/L. As the V_G lowers to its minimum value (approaching more negative V_G), the drain current increases because the negative potential on the sensing surface layer balances the negative built-up charges and thus attracts more holes from the Si channel, which compensates the width of the depletion region. When pH increases in the electrolyte, the concentration of the protons decreases in the solutions, hence there are fewer positive charges on the surface of the gate oxide which leads to less repulsion of the holes in the Si channel and as result, the depletion layer in Si decreases leading to more current flow [4]. The increase in pH can also be detected with the linear decrement of the threshold voltage [Fig. 6 inset] (positive values for p-type FET) of the sensing ISFET. A similar methodology can be used to design more accurate and complex biosensors with protein-peptide interactions.

IV.CONCLUSION

In conclusion, we have presented in this work, initial results based on the combination of numerical and analytical models which were developed to simulate high-aspect-ratio ISFET. Our results show that our methodology, which successfully combines numerical TCAD simulations and analytical models, computes the change of the device's current-volage characteristics as a function of pH values in the electrolyte. Moreover, a similar methodology can be used to significantly improve both analytical and numerical models to describe more complex nano-biosensors based on high-aspect-ratio FinFETs.

ACKNOWLEDGMENT

This project has received funding from the European Union's Horizon 2020 research and innovation program under grant agreement No 862539-Electromed-FET OPEN.

REFERENCES

[1] Sheehan, P.E. and L.J. Whitman, *Detection Limits for Nanoscale Biosensors.* Nano Letters, 2005. **5**(4): p. 803-807.

[2] Cui, Y., et al., *Nanowire Nanosensors for Highly Sensitive and Selective Detection of Biological and Chemical Species.* Science, 2001. **293**(5533): p. 1289.

[3] Nair, P.R. and M.A. Alam, *Performance limits of nanobiosensors.* Applied Physics Letters, 2006. **88**.

[4] Rollo, S., et al., *High Aspect Ratio Fin-Ion Sensitive Field Effect Transistor: Compromises toward Better Electrochemical Biosensing.* Nano Letters, 2019. **19**(5): p. 2879-2887.

[5] Rani, D., et al., *On the Use of Scalable NanoISFET Arrays of Silicon with Highly Reproducible Sensor Performance for Biosensor Applications.* ACS Omega, 2016. **1**(1): p. 84-92.

[6] Stern, E., Klemic, J.F., Routenberg, D.A., Wyrembak, P.N., Turner-Evans, D.B., Hamilton, and L. A.D., D.A., Fahmy, T.M., Reed, M.A., *Label-free immunodetection with CMOS-compatible semiconducting nanowires* Nature 445, 2007: p. 519–522.

[7] Gao, A., et al., *Silicon-Nanowire-Based CMOS-Compatible Field-Effect Transistor Nanosensors for Ultrasensitive Electrical Detection of Nucleic Acids.* Nano Letters, 2011. **11**(9): p. 3974-3978.

[8] Van Zeghbroeck, J., *Principles of Semiconductor Devices*. 2011: Bart Van Zeghbroeck.

[9] Robertson, J., *High dielectric constant oxides.* Eur. Phys. J. Appl. Phys., 2004. **28**(3): p. 265-291.

[10] Narang, R., M. Saxena, and M. Gupta, *Analytical Model of pH sensing Characteristics of Junctionless Silicon on Insulator ISFET.* IEEE Transactions on Electron Devices, 2017. **64**(4): p. 1742-1750.

[11] Valiskó, Mónika, Boda, Dezso, *The effect of concentration-and temperature-dependent dielectric constant on the activity coefficient of NaCl electrolyte solutions,* The Journal of Chemical Physics,2014,vol140

[12] van Hal, R.E.G., J.C.T. Eijkel, and P. Bergveld, A general model to describe the electrostatic potential at electrolyte oxide interfaces. Advances in Colloid and Interface Science, 1996. 69(1): p. 31-62.

[13] Medina-Bailon Cristina, Kumar Naveen, Dhar Rakshita P. Todorova, Ilina Lenoble, Damien Georgiev, Vihar P. García, César P., *Comprehensive Analytical Modelling of an absolute pH sensor*, Sensors Journal, 2021, Vol 21, Issue 15.

[14] Alam, M.A., *Principles of Electronic Nanobiosensors*. 2013.